Dual Additives Enabling High-Performance Solid Polymer Electrolytes for Stable Cycling of Lithium Metal Batteries

Mochun Zhang [a], Yuting Hu [a], Jing Xu [a], Junquan Lai [a], Jialong Cao [a], Mengran Wang [*a, b, c, d, e] and Yanqing Lai [a, b, c, e]

[a.] School of Metallurgy and Environment, Central South University, Changsha 410083, Hunan, China, E-mail: mengranwang93@163.com, laiyanqing@csu.edu.cn

[b.] Engineering Research Centre of Advanced Battery Materials, The Ministry of Education, Changsha 410083, Hunan, China

[c.] National Energy Metal Resources and New Materials Key Laboratory, Changsha, Hunan 410083, China

[d.] National Engineering Research Center of Advanced Energy Storage Materials, Changsha, Hunan 410083, China

[e.] Hunan Provincial Key Laboratory of Nonferrous Value-Added Metallurgy, Changsha, Hunan 410083, China

[*] Corresponding author

Email addresses: mengranwang93@163.com (Mengran Wang)

1.Experimental section

Materials

lithium bis(trifluoromethanesulfonyl)imide (LiTFSI, 99.9%), Vinyl ethylene carbonate (VEC, 99%), 2,2,2-trifluoroethyl methacrylate (TFEAMA, 98%), polyethylene glycol dimethacrylate (PEGDMA) crosslinker, 2,2'-Azobis(2methylpropionitrile) (AIBN), Copper fluoride (CuF_2, anhydrous), Lithium bis(oxalato)borate (LiBOB), N-methyl-2-pyrrolidone (NMP, 99.9%) were all purchased from Shanghai Aladdin Biochemical Technology Co., Ltd. Glass fiber (Whatman GF/C) seperators were procured from Duoduochem. Carbon black and PVDF (99.5%) were obtained from Taiyuan Liyuan Lithium Technology Center. lithium cobalt oxide (LCO) was sourced from the Shenzhen Kejing Star Technology Co., Ltd. All the materials were stored in an Ar-filled glove box (H_2O < 0.1 ppm, O_2 < 0.1 ppm).

Preparation of PVT electrolyte

A specified amount of VEC, TFEMA, PEGDMA (crosslinker), and LiTFSI was weighed and transferred into a glass vial, which was placed on a magnetic stirrer for approximately 30 minutes. After stirring, AIBN (thermal initiator, 1.0 wt.% relative to the total mass of the two monomers) was added, followed by an additional 10 minutes of stirring to obtain the precursor solution. The prepared solution was injected into a cell, which was then heated at 80°C for 8 hours and 60°C for 16 hours. After polymerization, the cell was allowed to cool to room temperature for at least 1 hour before performance testing.

Preparation of PVT-C electrolyte

Building on the PVT polymer electrolyte, varying amounts of copper fluoride (0.25 wt.%, 0.5 wt.%, 0.75 wt.%, and 1.0 wt.%, relative to the combined mass of the two monomers VEC and TFEMA) were added and stirred for at least 8 hours. Once copper fluoride was fully dissolved, azodiisobutyronitrile (AIBN, thermal initiator, 1.0 wt.% relative to the total mass of VEC and TFEMA) was introduced, and the mixture was stirred for an additional 10 minutes to yield the precursor slurry.

Preparation of PVT-CB electrolyte

For the PVT-C polymer electrolyte, different amounts of LiBOB (0.5 wt.%, 1.0 wt.%, 1.5 wt.%, and 2.0 wt.% relative to the total mass of the two monomers VEC and TFEMA) were incorporated and

stirred for at least 8 hours. After CuF_2 and LiBOB were completely dissolved, AIBN (1.0 wt.% relative to the total mass of the two monomers) was added, and the precursor slurry was obtained after an additional 10 minutes of stirring.

Materials characterization

In situ Fourier transform infrared spectroscopy (FTIR) was employed to analyze the functional group changes of the electrolytes before and after polymerization, enabling the assessment of polymerization success. FTIR measurements were conducted using a Nicolet iS50 instrument (Thermo Fisher Technology), with an infrared spectral range of 400–4000 cm^{-1}. Both the monomer and the prepared solid electrolyte were tested in a room temperature air atmosphere.

Thermogravimetric analysis (TGA) was used to investigate the thermal stability of the solid electrolytes. The thermal analysis was performed using an STA 449 F5 Jupiter instrument (Nez Instrument Manufacturing, Germany) with a test temperature range of 30–600 °C, a heating rate of 10 °C min^{-1}, and a nitrogen atmosphere.

X-ray diffraction (XRD) was employed to determine the crystallinity of the solid electrolyte. XRD measurements were carried out with a Rui Ying 2Empyrean 2 instrument (PANalytical, Netherlands) using a copper target, with an angle range of 10° to 80° and a sweep speed of 10° min^{-1}.

Differential scanning calorimetry (DSC) was utilized to measure the glass transition temperature (Tg) of the polymer solid electrolyte. The DSC analysis was performed using a Mettler DSC3 instrument (Mettler Toledo, Switzerland), under nitrogen atmosphere, with a heating rate of 5 °C min^{-1} and a temperature range from −80 to 200 °C, without insulation.

Scanning electron microscopy (SEM) was used to examine the microstructure of the polymer solid electrolyte and electrode plates. An energy dispersive X-ray spectrometer (EDS) was also employed to investigate the elemental distribution on the surface of materials through point scanning, line scanning, and surface scanning. The SEM instrument used was a TESCAN CLARA model.

Transmission electron microscopy (TEM) was used to observe the ultrastructure of the materials, particularly the active material properties of the recycled lithium cobalt oxide electrode. The TEM measurements were conducted with a JEM-F200 instrument (JEOL, Japan).

X-ray photoelectron spectroscopy (XPS) was used to analyze the chemical states and molecular structures of elements on the material's surface, particularly to examine the composition of the

interface layer on the cathode and anode after cycling. The XPS analysis was performed using an ESCALAB 250Xi instrument (Thermo Fisher Scientific).

Electrochemical characterization

The steel symmetric battery was assembled in a glove box, and electrochemical impedance spectroscopy (EIS) was conducted using a Gamry intrument to measure the impedance of the battery. Afterward, the steel symmetric battery was disassembled, and the thickness of the in-situ polymerized solid electrolyte film was measured. The ionic conductivity (σ) of the electrolyte was then calculated using the following formula:

$$\sigma = \frac{L}{RS}$$

Where the σ represents the ion conductivity of electrolyte, L is the thickness of electrolyte, R is the impedance, and S is the effective area of the electrolyte.

The activation energy is the energy barrier that lithium ions must overcome during internal migration within the battery. The ion conductivity (σ) of different temperatures was fitted into the Arrhenius model to calculate the activation energy (E_a) of PVT, PVT-C and PVT-CB electrolytes. The formula is as follows:

$$\sigma(T) = Aexp(-\frac{E_a}{RT})$$

Where E_a is the activation energy, A is the pre-exponential factor, and R is the ideal gas constant (8.314 J mol^{-1} K^{-1})

The calculation of lithium-ion transference number (t_{Li+}) was determined by assembling lithium symmetric batteries Li|SPEs|Li. Chronoamperometry was performed by applying a constant voltage of 10 mV, and the impedance in the frequency range of 0.1 Hz to 1 MHz was recorded before and after the test. The lithium-ion transference number was calculated using the following formula:

$$t_{Li^+} = \frac{I_{SS}(\Delta V - I_0 R_0)}{I_0(\Delta V - I_{SS} R_{SS})}$$

Where ΔV is the polarization voltage, I_0 and I_{SS} represent the initial and steady-state currents, and R_0 and R_{SS} are the interfacial impedances before and after polarization, respectively.

To evaluate the interfacial stability of the electrolytes with the electrodes, batteries based on

SS|SPE|Li were tested using linear sweep voltammetry (LSV). The voltage sweep was applied from 3 V to 6 V at a sweep rate of 1 mV s^{-1}.

The galvanostatic charge-discharge performance of the batteries based on Li|SPEs|Li was tested using a LAND battery test system with a current density of 0.1 mA cm^{-2}. Additionally, to evaluate the stripping and deposition behavior of the lithium metal anode, tests were conducted at different current densities. For the Li|SPEs|LCO batteries, the cycling stability was assessed with charge and discharge voltages set between 3.0 and 4.4 V, using the same LAND battery test system.

Computational method

All quantum chemical calculations were carried out using dmol3 software package based on density functional theory (DFT) method. The B3LYP functional were adopted for all the geometry optimizations. The SCF tolerance was set to 1×10^{-6} hartree. In the process of geometry optimization, all atomic coordinates were relaxed without any limitation. The maximum force is 0.002 hartree/Å, max atom displacement is 0.005 Å and max-energy difference is 1×10^{-5} hartree/atom.

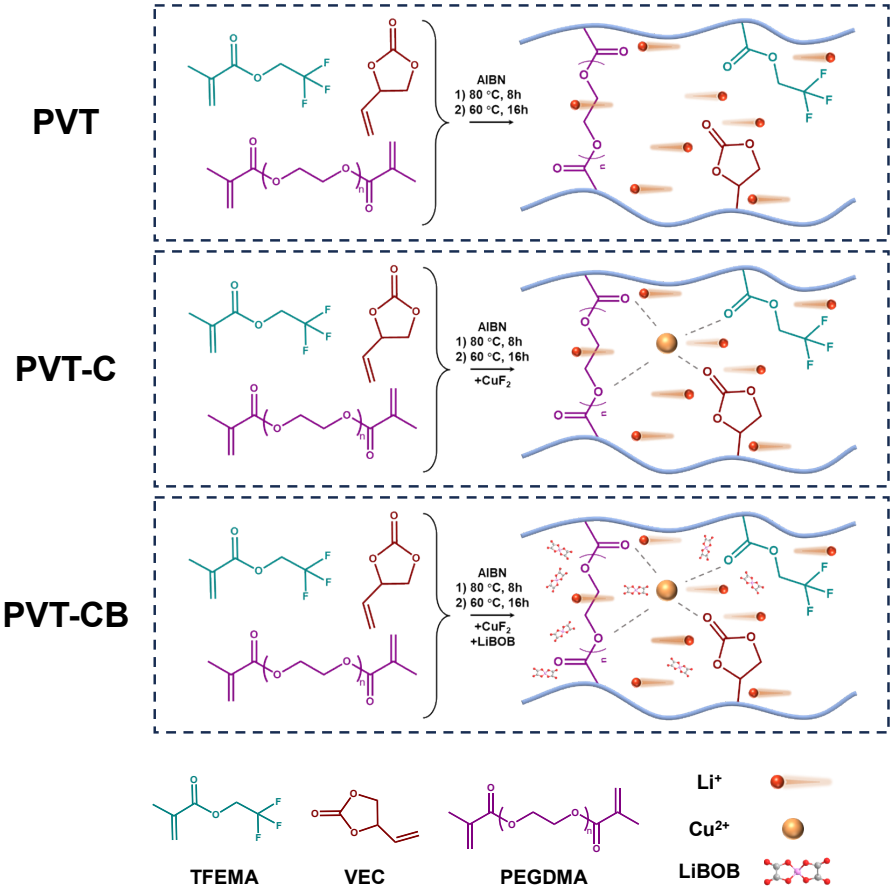

Fig. S1 Synthesis diagram of three polymer electrolytes.

Fig. S2 Optical images of PVT-CB and PVT-C polymer electrolytes under folding and recover states.

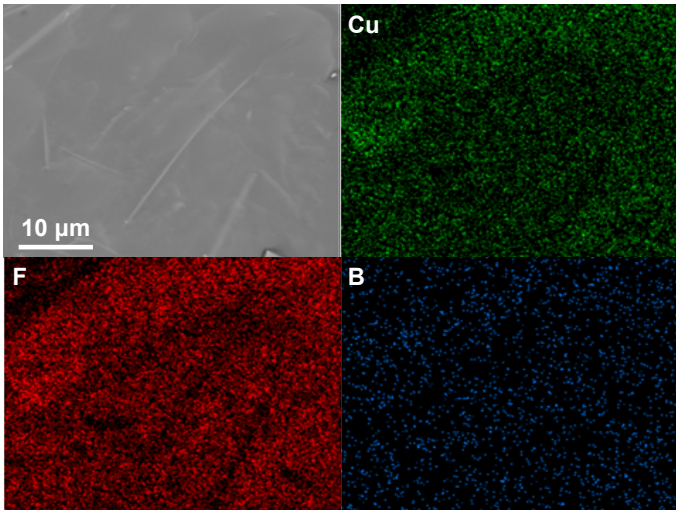

Fig. S3 The SEM image and the corresponding EDS mappings of PVT-CB electrolyte.

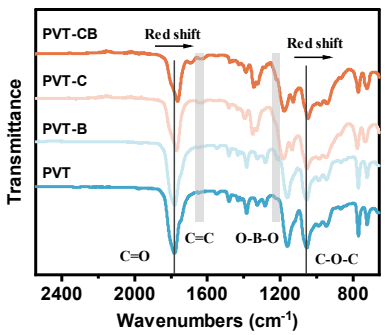

Fig. S4 The FTIR spectra of PVT, PVT-B, PVT-C and PVT-CB electrolytes without LiTFSI.

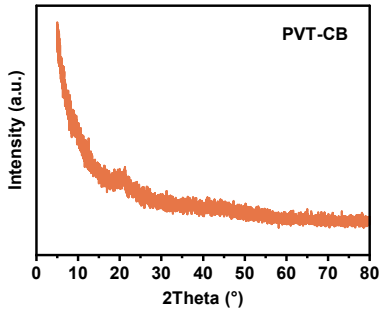

Fig. S5 The XRD spectra of PVT-CB electrolyte.

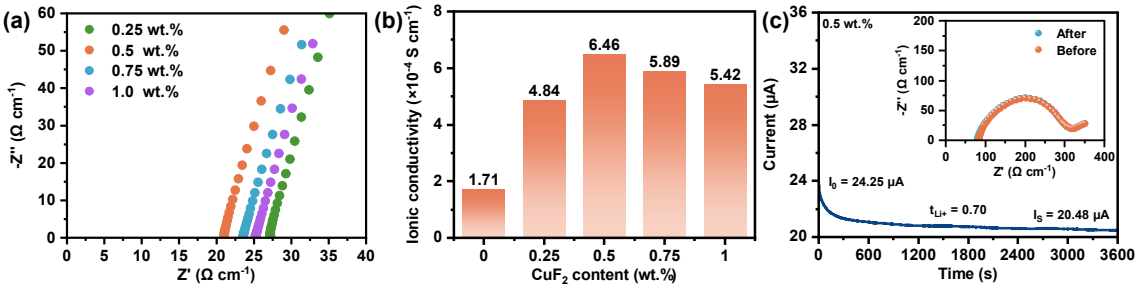

Fig. S6 (a) Impedance spectra and (b) ionic conductivity diagrams (25 °C) of PVT-C with different CuF_2 contents. (C) Li-ion transference number of PVT-C.

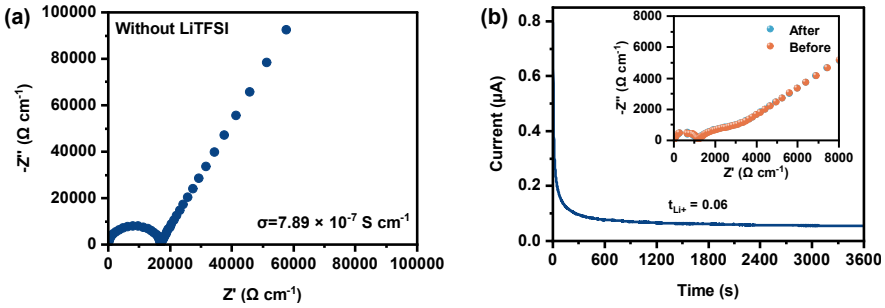

Fig. S7 (a) Conductivity and (b) Li-ion transference number of PVT-C without LiTFSI.

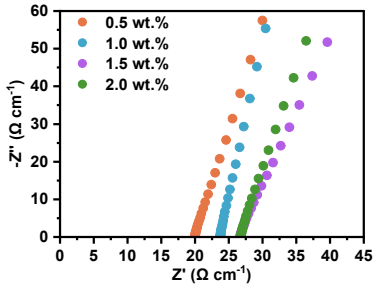

Fig. S8 Impedance spectra of PVT-CB with different LiBOB contents.

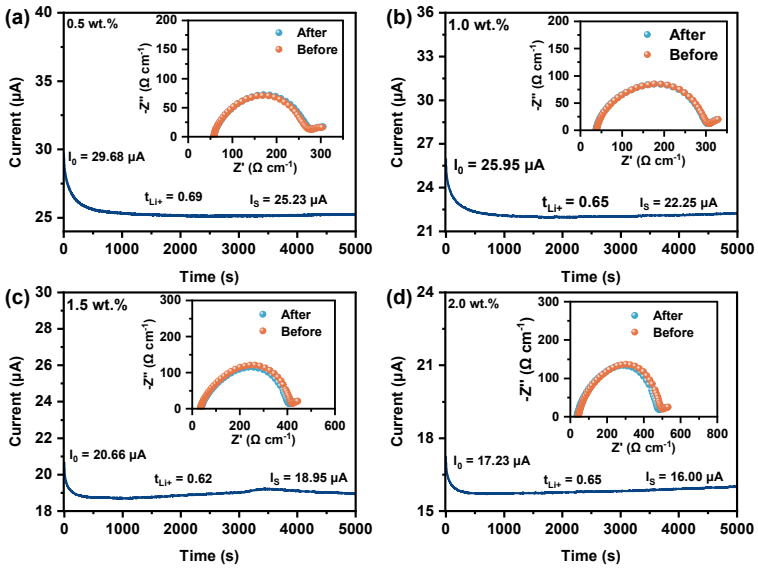

Fig. S9 The ionic transfer number of PVT-CB electrolyte with different LiBOB contents. (a) 0.5 wt.%, (b) 1.0 wt.%, (c) 1.5 wt.%, (d)2.0 wt.%.

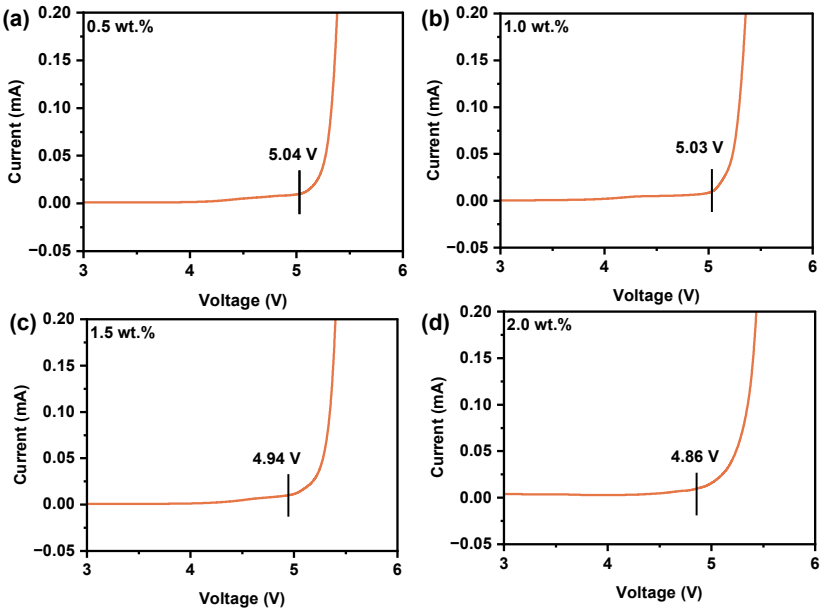

Fig. S10 LSV cruves of PVT-CB electrolyte with different LiBOB contents. (a) 0.5 wt.%, (b) 1.0 wt.%, (c) 1.5 wt.%, (d) 2.0 wt.%.

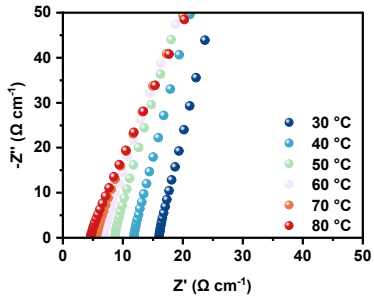

Fig. S11 EIS curves of PVT-CB with varying temperatures.

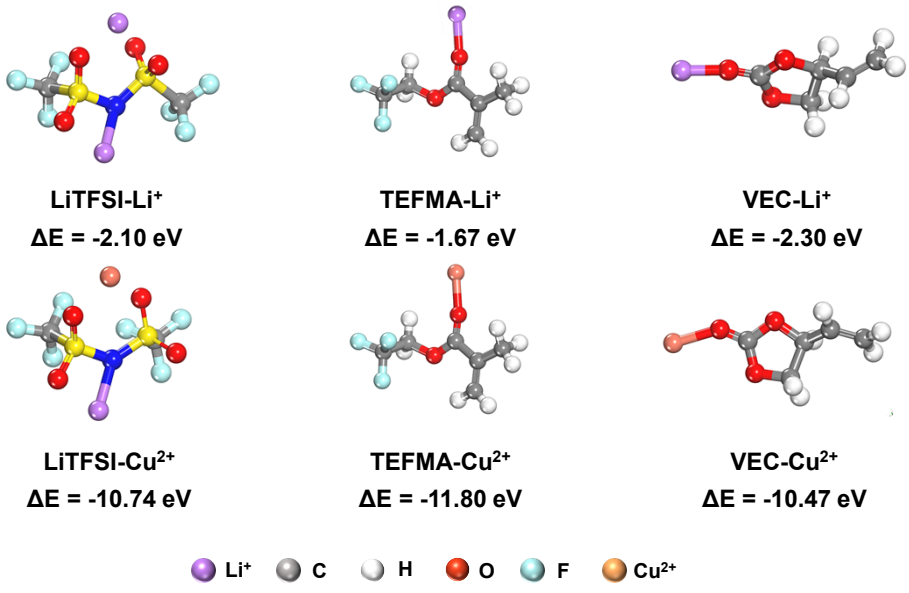

Fig. S12 Structures and binding energies of LiTFSI-Li^+/Cu^{2+}, TFEMA-Li^+/Cu^{2+}, and VEC-Li^+/Cu^{2+} calculated by DFT. Among them, the binding energy of VEC-Li^+ and FEMA-Li^+ can be referred to our previous work[1].

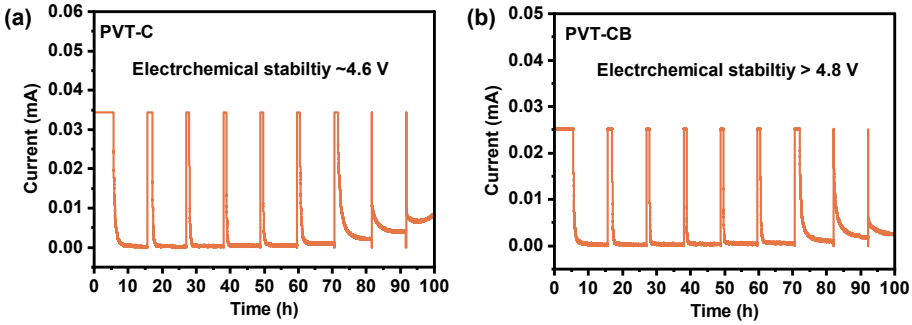

Fig. S13 Leakage current tests on Li|PVT-C|LCO and Li|PVT-CB|LCO.

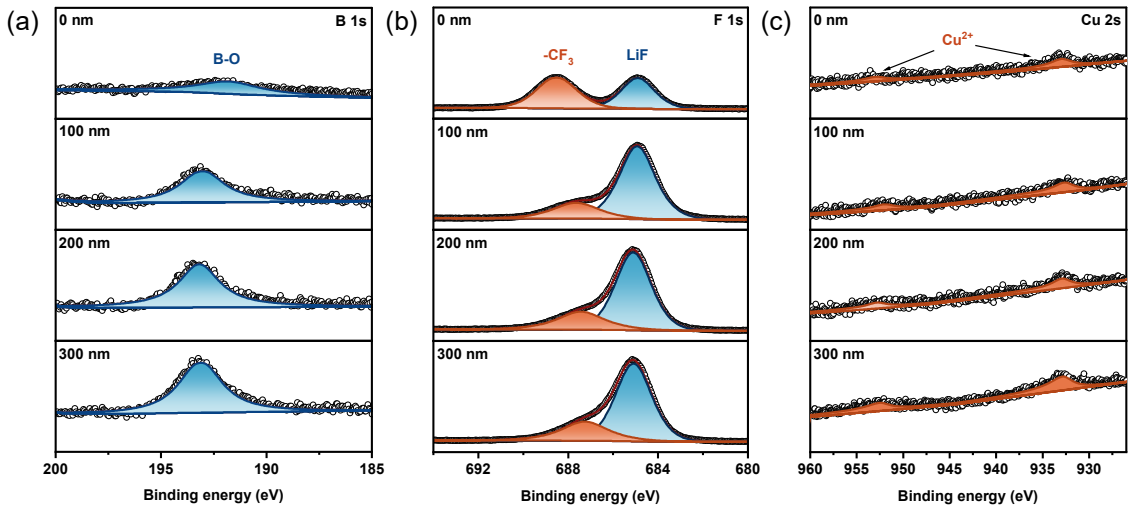

Fig. S14 XPS depth profiles with different sputtering time of (a) B 1s, (b) F 1s and (c) Cu 2p in Li metal with PVT-CB after 100 h cycles.

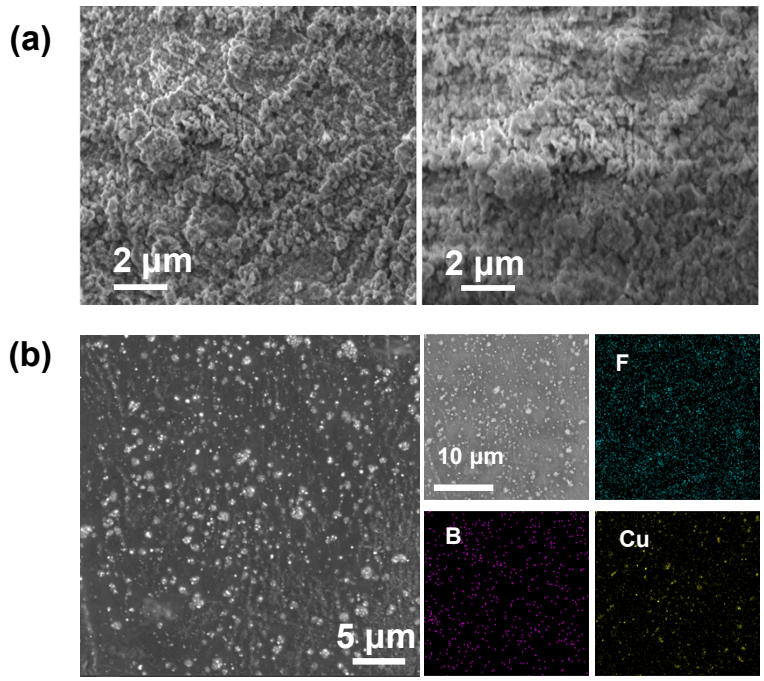

Fig. S15 (a) The SEM image of Li metal in Li|PVT|LCO battery after cycled. (b) The SEM image and the corresponding EDS mappings of Li metal in Li|PVT-CB|LCO battery after cycled.

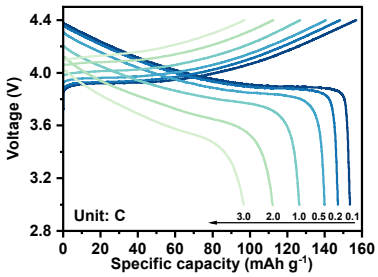

Fig. S16 Charge-discharge voltage profiles at various rates of the Li|PVT-C|LCO battery.

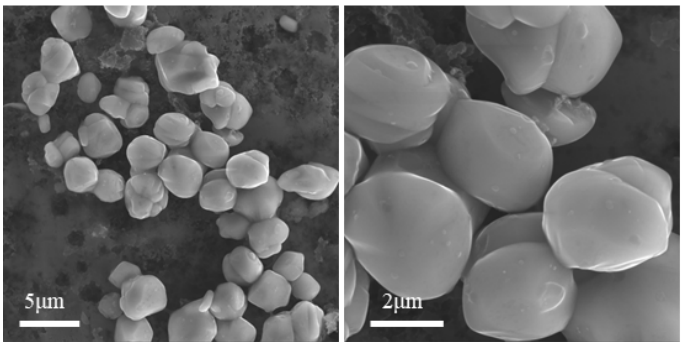

Fig. S17 SEM images of LCO materials in Li|PVT-CB|LCO battery after cycled.

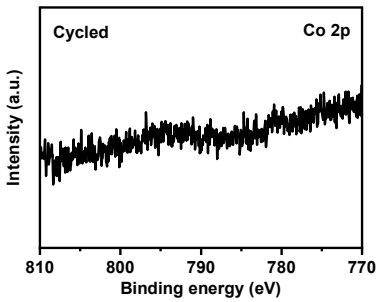

Fig. S18 XPS profile of Co 2p in Li metal with PVT-CB electrolyte and LCO cathode after cycled.

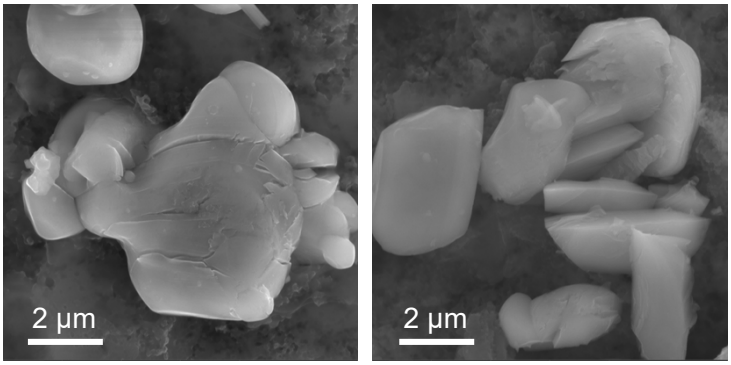

Fig. S19 SEM images of LCO materials in Li|PVT-C|LCO battery after cycled.

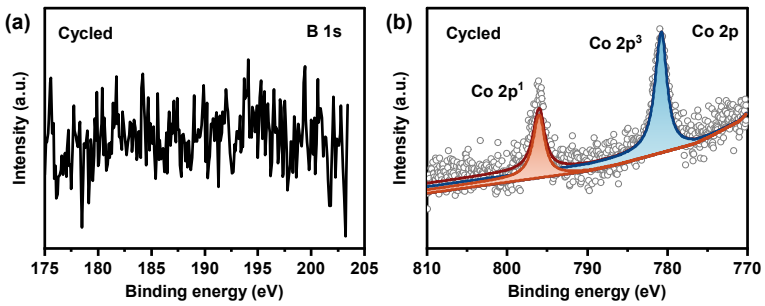

Fig. S20 XPS profile of (a) B 1s in LCO cathode and (b) Co 2p in Li metal with PVT-C electrolyte after cycled.

Table S1. Comparison of electrochemical performance of PVT-CB electrolyte in comparison with other reported polymer electrolytes in Li|LCO battery.

Name	Voltage window	Capacity retention	Rate	Number of cycles	Ref.
CSE-5	3.0-4.5 V	94%	0.1C	200	2
PAL	3.0-4.3 V	81%	1C	300	3
PEO-cPTFBC-LiDFOB	3.0-4.35 V	73.8%	0.1C	50	4
p-MDE-S	2.5-4.3 V	91.6%	0.5C	50	5
C-SPE	3.0-4.5 V	83.9%	1C	200	6
VEC-HEMA	3.0-4.2V	93.5%	0.1C	100	7
P(VEC_1-$CEA_{0.3}$)/LiTFSI@CE	3.0-4.45 V	88.5%	0.2C	160	8
PVT-CB	**3.0-4.4 V**	**88.8%**	**0.5C**	**250**	**This work**

Reference

1. J. Xu, Y. Hu, M. Zhang, et al., *ACS Appl. Energy Mater.*, 2024, **7**, 10777-10783.
2. Y. Wang, L. Wu, Z. Lin, et al., *Nano Energy*, 2022, **96**, 107105.
3. L. Wu, Y. Wang, M. Tang, et al., *Energy Storage Mater.*, 2023, **58**, 40-47.
4. Q. Wang, X. Liu, Z. Cui, et al., *Electrochim. Acta*, 2020, **337**, 135843.
5. M. Zhang, C. Lei, T. Zhou, et al., *ACS Appl. Mater. Interfaces*, 2022, **14**, 55653-55663.
6. J. Liu, Y. Zhang, H. Ji, et al., *Adv. Sci.*, 2022, **9**, e2200390.
7. Y. Huang, Z. Xie, W. Zhu, et al., *ACS Appl. Polym. Mater.*, 2024, **6**, 3624-3636.
8. S. Ma, Y. Zhang, D. Zhang, et al., *J. Energy Chem.*, 2024, **98**, 422-431.